Tailoring Electrolyte Coordination Structure for High-Rate Polymer-Based Solid-State Batteries

Zexi Wang[1], Zhencheng Huang[1], Hao Guo[2], Tao Huang[1,3] , Jingguo Gao[1,3,4], Junzheng Lai[1,3], Na Feng[1,3], Ziqi Wang[5], Xuming Yang[1,3], Yongliang Li[1], Jianhong Liu[1,3], Yi Wang[1]*Qianling Zhang[1,3,4], Jiangtao Hu[1,3,4]*, Xiangzhong Ren[1]*

[1] Shenzhen Key Laboratory of Functional Polymers, College of Chemistry and Environmental Engineering, Shenzhen University, Shenzhen, 518060, China

[2] State Key Laboratory of Advanced Chemical Power Sources, Zunyi, Guizhou, 563003, China

[3] Graphene Composite Research Center, College of Chemistry and Environmental Engineering, Shenzhen University, Shenzhen, 518060, China

[4] State Key Laboratory of Intelligent Construction and Healthy Operation and Maintenance of Deep Underground Engineering, Shenzhen University, Shenzhen 518060, China

[5] Department of Materials Science and Engineering, College of Chemistry and Materials Science, Jinan University, Guangzhou, 511443, China

***Corresponding author**: zhql@szu.edu.cn, hujt@szu.edu.cn, renxz@szu.edu.cn

Supporting Information

Experimental section

Materials

N, N-Dimethylformamide (DMF) was purchased from Aladdin. PVDF-HFP (M_w=600,000, Solef, 21216) was purchased from Shanghai Aichun Biotechnology Co., Ltd. LATP was purchased from Shenzhen Kejing Star Technology Co., Ltd. MOF808 was prepared according to previous literature[1, 2]. $LiBF_4$ (99.99%) and LiTFSI (99.99%) were purchased from Shanghai Aladdin Biochemical Technology Co., Ltd. All the above salt were used after drying at 80 ℃ in a vacuum for 12 hours. Triethyl phosphate (TEP, 99.8%) and fluoroethylene carbonate (FEC, 99.9%) were bought from the DodoChem Co., Ltd. All the above solvents were dehydrated by molecular sieves (3 Å, Aladdin).

Preparation of the CPEs membrane

First, 0.2 g of PVDF-HFP, 0.1 g of LATP, 0.1 g of LiTFSI and 0.06 g of $LiBF_4$ were dissolved in 5 mL of DMF and magnetically stirred at room temperature for 24 h to obtain a white transparent solution. Afterward, the MOF808 nanoparticles with the weight percentage of 0 wt%, 1 wt%, 3 wt% and 5 wt% in the total amount of PVDF-HFP were added into the above solution with ultrasonic processing of 30 min, followed by mechanical stirring at room temperature for 12 h to obtain a homogeneous suspension. Subsequently, the suspension was dried at 60 °C with a vacuum for 20 h to form the solid-state electrolytes by the solution casting method. Before use, the obtained electrolyte films were cut into wafers of a 18 mm diameter and kept in a glove box with Ar; named PL, PLM-1, PLM-3, PLM-5, respectively.

Fabrication of cells

The single crystal $LiNi_{0.83}Co_{0.12}Mn_{0.05}O_2$ (SC-NCM83) powders was bought from the GEM (Wuxi) Energy Material Co., Ltd. Conductive carbon black (Super P) and poly(vinylidene difluoride) (PVDF) were obtained from the Hefei Kejing Material Technology Co., Ltd. The Nmethyl-2-pyrrolidone (NMP) was purchased from Shanghai Aladdin Biochemical Technology Co., Ltd. The cathode was prepared by mixing SC-NCM83, Super P and PVDF with a mass ratio of 8:1:1 in NMP. Then, the slurry was coated onto an aluminum current collector. Finally, the NMC electrodes was dried at 110 ℃ in a vacuum for 20 h before using them. The electrodes were cut into small circles with a 13 mm diameter, and the mass loading of active material was approximately 2.5 mg cm^{-2}.

For the electrochemical tests, 5 μL liquid electrolyte (1.5 M $LiBF_4$ in TEP:FEC=3:1 in vol%) was dropped to the surface of the electrolyte films to wet the interface and plasticize the electrolytes in an Ar-filled glovebox.

Materials Characterization

The X-ray diffraction (XRD) measurements of the CPEs were characterized on a Rigaku D/max-2500 advanced X-ray diffractometer with Cu Kα radiation. Morphological and structural analyses were performed by scanning electron microscope (SEM, SM-7800F), with energy dispersive spectroscopy (EDS) and transmission electron microscope (TEM, JEM-2100). The chemical component and valence state were analysed by X-ray photoelectron spectroscopy (XPS, Thermo Scientific Escalab 250X, USA) measurement. The thermal stability was investigated by thermogravimetric analysis (TGA, METTLER) and differential scanning calorimetry (DSC, NETZSCH) with a heating rate of 10 °C min^{-1} and the range from 25 to 600 °C under Ar atmosphere. The Raman spectra (Thermo Fisher Renishaw) were employed at the range of 690-790 cm^{-1} with 532 nm lasers. The stress-strain tests of the CPEs were carried out using an INSTRON 5565 to obtain the mechanical strength. The Fourier-transform infrared (FTIR) spectra were executed by FTIR spectroscope (IR Affinity-1) with a wavenumber range of 4000-450 cm^{-1} and a resolution of 1.0 cm^{-1} in an attenuated total reflection (ATR) mode. In situ electrochemical impedance spectroscopy (EIS) tests were performed on an electrochemical workstation (Solartron, USA) and 2032-coin cells. The distribution of relaxation time (DRT) transformations were executed with the aid of MATLAB software, and it was ensured that all parameters remained constant throughout the computational process to maintain the uniformity of the DRT outcomes. The charge/discharge voltages were in the range of 2.7-4.3 V with 0.2 C. The EIS tests were performed in the frequency range of 100000 Hz to 0.01 Hz with an amplitude of 10 mV.

Electrochemical measurements

The ionic conductivities of PLM-3 and PL were measured by electrochemical impedance spectroscopy (EIS) from 100 kHz to 1 Hz with a 5 mV AC oscillation. Prior to the EIS measurements, the cells were kept at each test temperature for 1 h to reach the thermal equilibrium. The ionic conductivities (σ) were calculated following equation S1:

$$\sigma = \frac{L}{RS} \tag{S1}$$

where L is the thickness of the electrolyte, R is obtained by EIS measurement with stainless steel symmetric cells, and S is the area of stainless steel. The activation energy was calculated from the Arrhenius equation S2:

$$\sigma = Aexp(-\frac{E_a}{RT}) \tag{S2}$$

where A and E_a is the pre-exponential factor and the activation energy of ions transportation, respectively. R represents the molar gas constant, and T represents the absolute temperature.

The Li/Li symmetric cells were assembled and polarized by a voltage (ΔV=10 mV) for 5000 s to test the lithium transference number t_{Li+}. At the same time, EIS measurement as well as initial and steady-state of Li/Li symmetric cells was performed from 100 kHz to 0.01 Hz with a 5 mV AC oscillation. t_{Li+} is calculated based on the following equation S3:

$$t_{Li+} = \frac{I_s(\Delta V - I_0 R_0)}{I_0(\Delta V - I_s R_s)} \tag{S3}$$

where I_s and I_0 is the steady-state currents and initial current, respectively, R_s and R_0 is the interfacial resistance after and before polarization, respectively.

The LSV curves were examined from open circuit voltage to 6 V versus Li/Li^+ at a scanning rate of 1 mV s^{-1} using an electrochemical workstation (CHI660E, Chenhua Co., Ltd). Galvanostatic charge/discharge tests of cells were performed on LAND CT2001A test systems. The cycled cells were transferred into a glovebox and dissembled for further examination. The SC-NCM83 cathode and lithium metal anode were transferred into a chamber with a sealed Ar-filled vessel for SEM and XPS examination. The full cells underwent testing at a rate of 0.33 C, 0.5 C or 2 C within a voltage window of 2.7 to 4.3 V. The rate capability was assessed using identical charging and discharging rates, which were 0.1 C, 0.2 C, 0.5 C, 1 C, 2 C and 5 C. The LAND CT2001A testing apparatus was employed to record the electrochemical performances. In this context, a 1C rate is equivalent to a current density of 200 mA g^{-1}.

Computational Details

(1) MD simulations were performed in GROMACS using the General Amber Force Field (GAFF). Topology files and bonded and Lennard-Jones parameters were generated by using the Autoff while

the RESP atomic charges from Multiwfn3.8 program were used[3]. The cutoff for the Lennard-Jones potential was set to 12 Å. The long-range Coulombic interactions were counted by a particle–particle particle-mesh. The initial periodic systems were set up using PACKMOL[4]. All ions and molecules were inserted in an initial cube box with 8 nm sides. In the equilibrium stage of the system, the energy of the simulated system was minimized by the conjugate gradient method first, then the equilibrium simulation was carried out under NPT ensemble for 10 ns. Finally, the simulation was continued for 20 ns with NVT ensemble and data were collected. Only the final 10-ns trajectory was sampled for the analysis of radial distribution function and solvent-solute interaction environments.

(2) DFT: All the molecules were first optimized using Gaussian with the three-parameter empirical formulation B3LYP for the exchange-correlation density-functional energy in conjunction with the basis set of 6-311+G(d,p). A dispersion correction was also considered using the Becke-Johnson damping function. The solvent-solute interaction was considered with the universal solvation model of SMD[5]. Frequency analysis was performed to ensure the ground state of molecular structures.

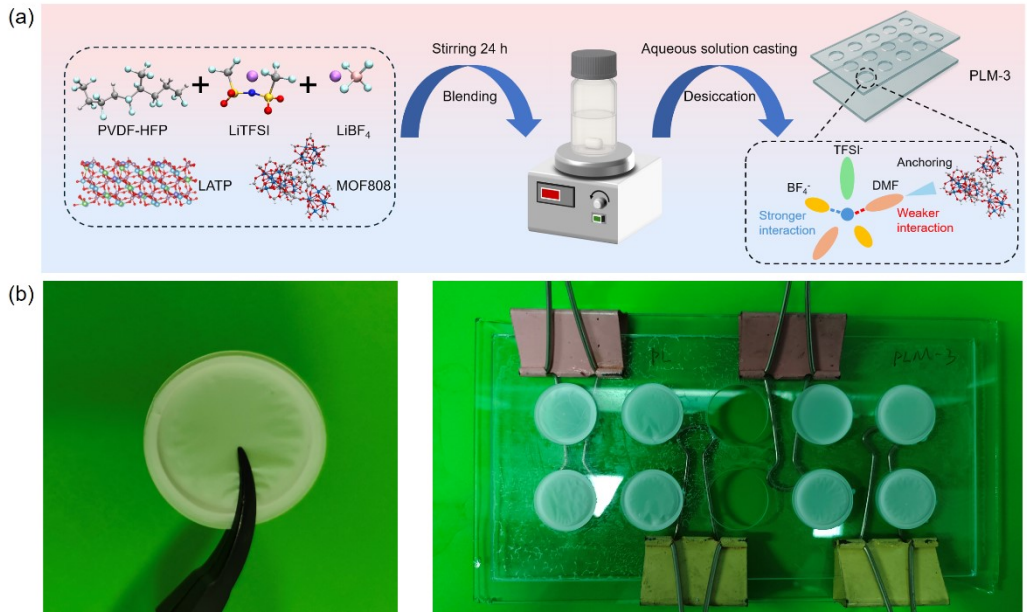

Figure S1. (a) Preparation processes of the CPEs film. (b) Optical photographs of the PLM-3 electrolyte.

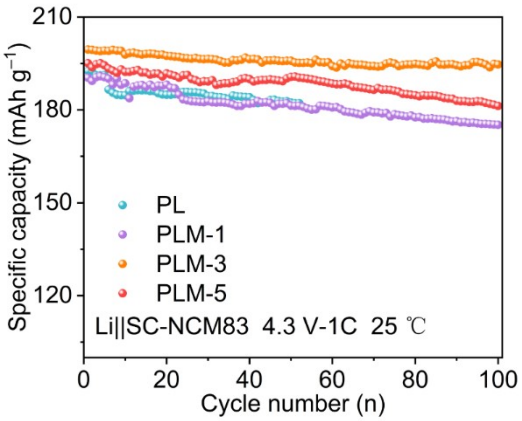

Figure S2. Cycling performance of SC-NCM83/CPEs/Li cells at 1 C between 2.7-4.3 V.

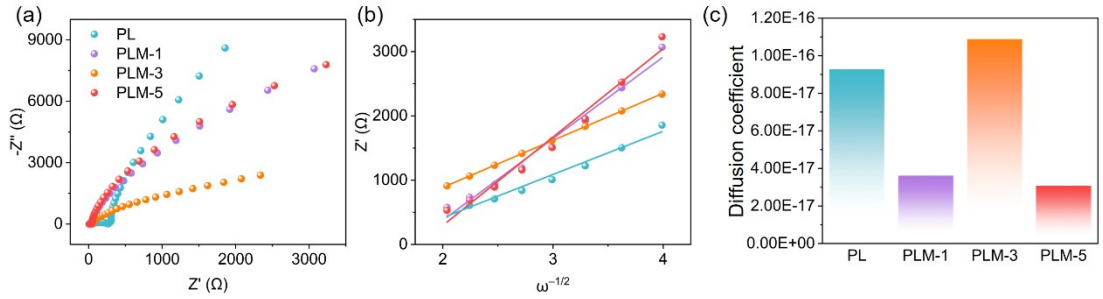

Figure S3. (a) AC impedance spectra of uncycled SC-NCM83/Li cells from different samples. (b) According to the standard Warburg impedance method for fitting of (a). (c) Diffusion coefficient of different samples.

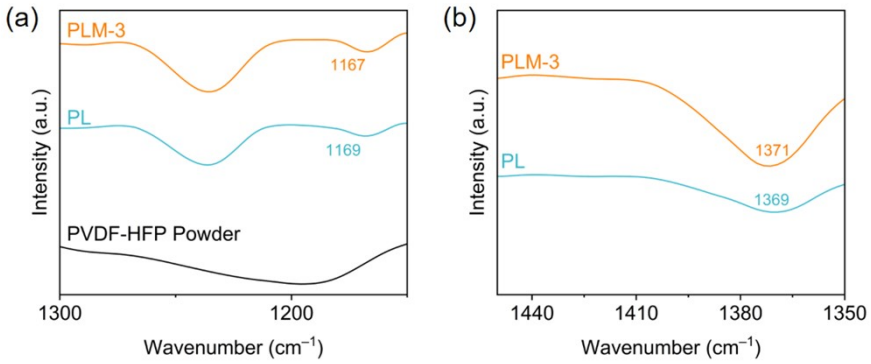

Figure S4. (a, b) Locally enlarged image of FT-IR spectra in **Figure 1a**.

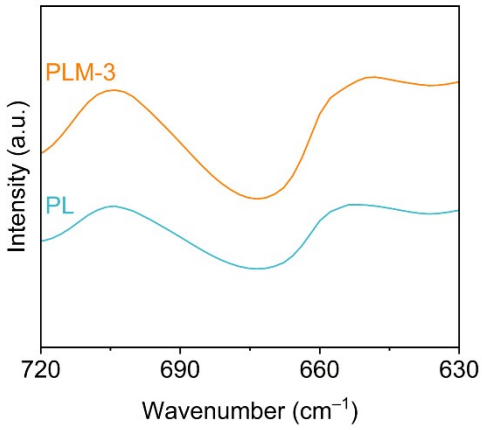

Figure S5. FT-IR spectra of PL and PLM-3 electrolytes.

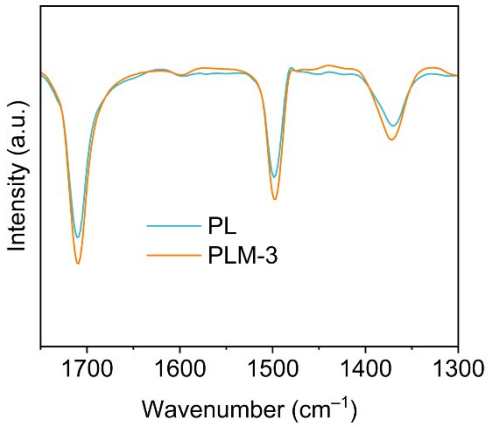

Figure S6. FT-IR spectra of PL and PLM-3 electrolytes on the same scale.

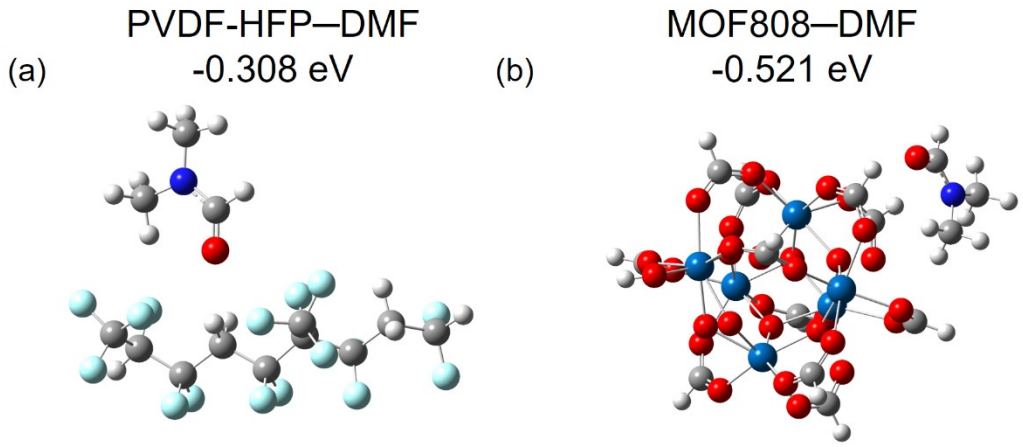

Figure S7. DFT calculation results of adsorption energy. (a) DMF with PVDF-HFP. (b) DMF with MOF808.

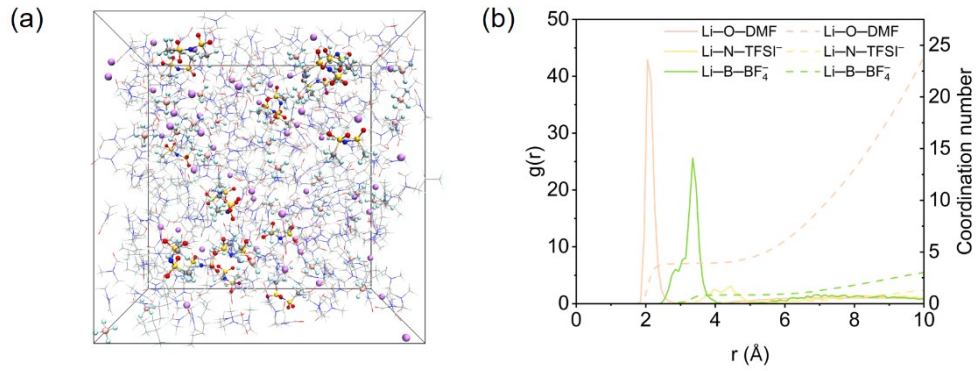

Figure S8. (a) MD simulation snapshots of PL electrolyte. (b) The radial distribution functions (g(r)) and coordination number (CN) of PL electrolyte. The solid lines represent g(r) and the dashed lines represent CN.

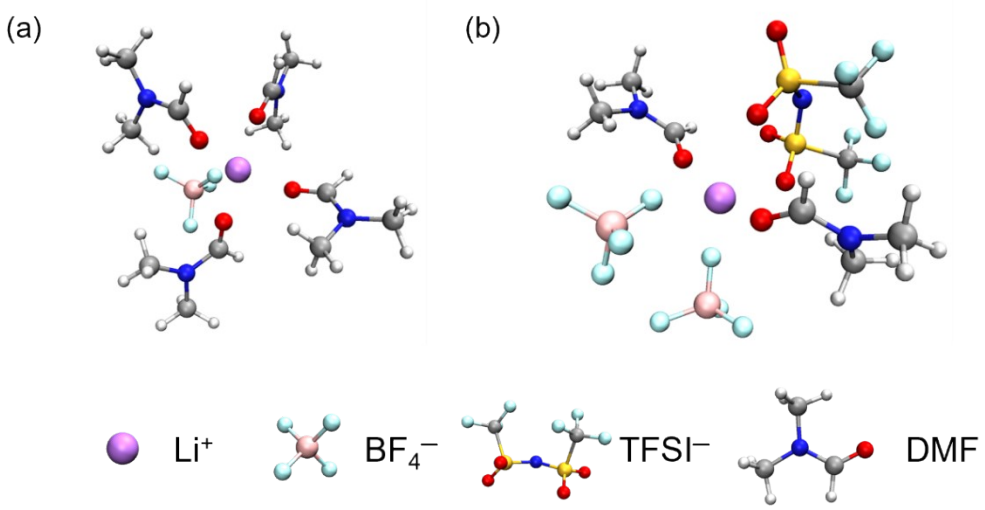

Figure S9. Snapshots of the solvation structure of (a) PL electrolyte and (b) PLM-3 electrolyte.

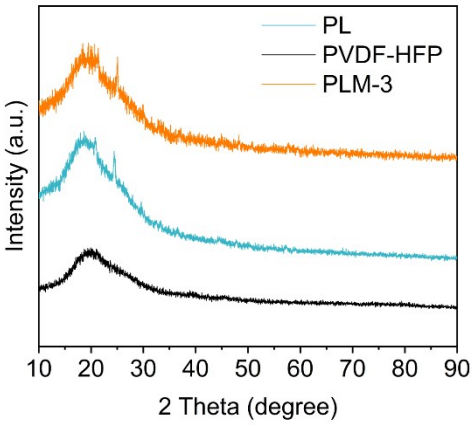

Figure S10. XRD patterns of the PVDF-HFP, PL and PLM-3 electrolytes.

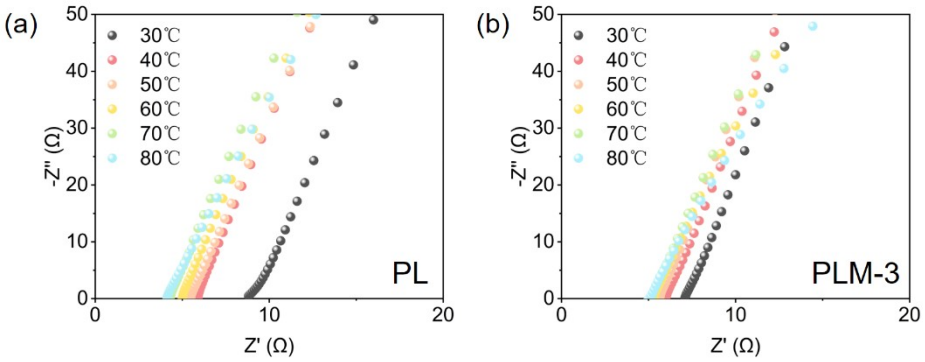

Figure S11. Nyquist plots of PL electrolyte (a) and PLM-3 electrolyte (b) at different temperatures.

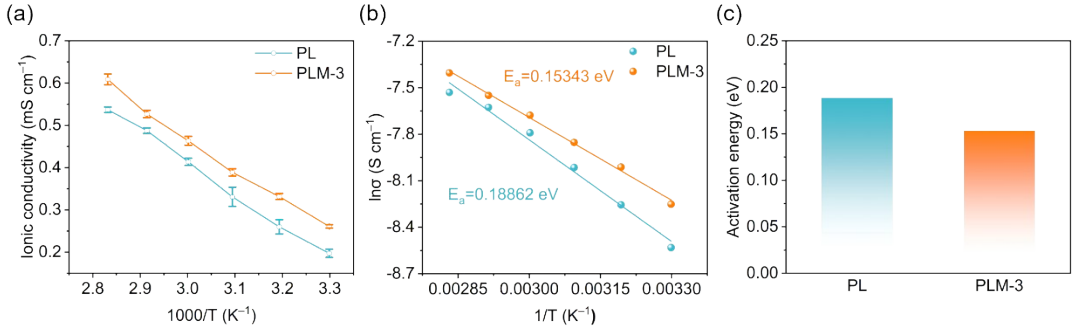

Figure S12. (a) Ionic conductivities with error bars of different samples at different temperatures. (b) Arrhenius plots of the ionic conductivities of PL and PLM-3 electrolytes. (c) Activation energy of PL and PLM-3 electrolytes.

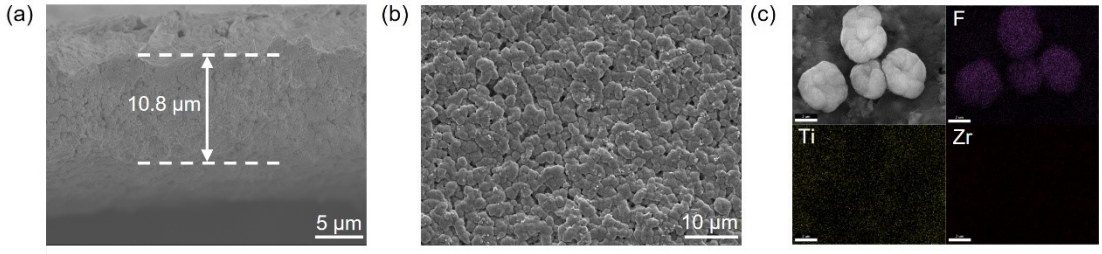

Figure S13. (a) Cross-sectional and (b) surface SEM images of PL electrolyte. (c) Surface energy dispersive spectroscopy (EDS) mappings of F, Ti and Zr element in the PL electrolyte.

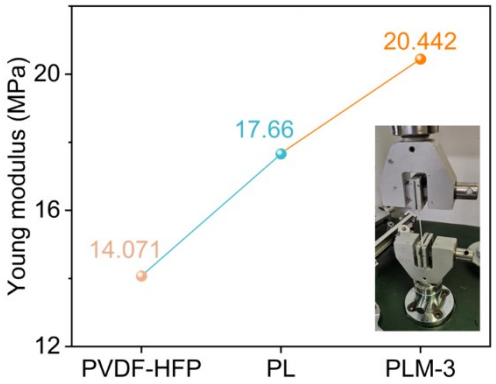

Figure S14. Young modulus plot of PVDF-HFP, PL and PLM-3 electrolytes (Inset is an optical photograph of the tensile test instrument).

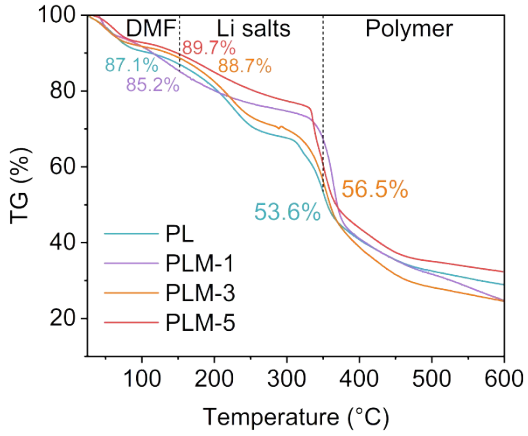

Figure S15. TGA curves of different electrolytes.

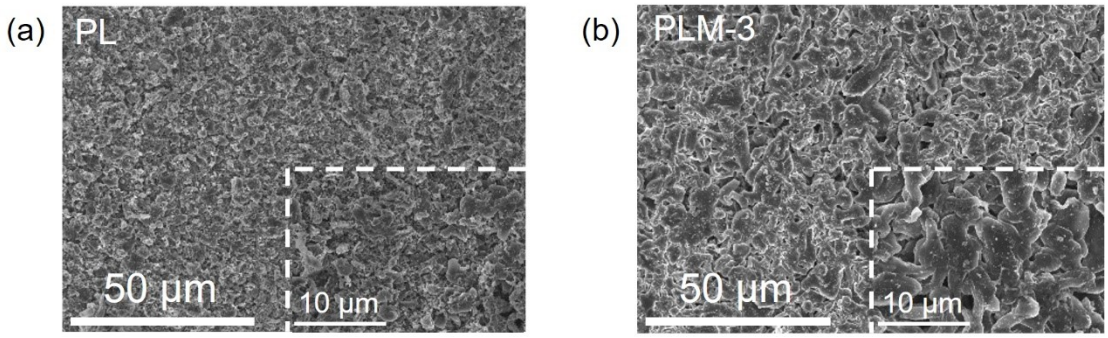

Figure S16. (a, b) Morphological evolution of Li deposition on Cu current collector using PL and PLM-3. The areal capacity from the counter Li metal electrode is 5 mAh cm^{-2}.

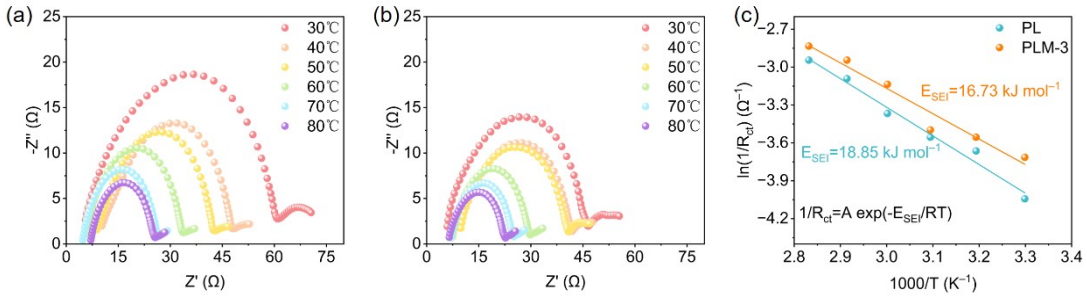

Figure S17. EIS results of fresh symmetric Li||Li cells using (a) PL and (b) PLM-3 at different temperatures. (c) Arrhenius behavior of Li^+ desolvation PL and PLM-3.

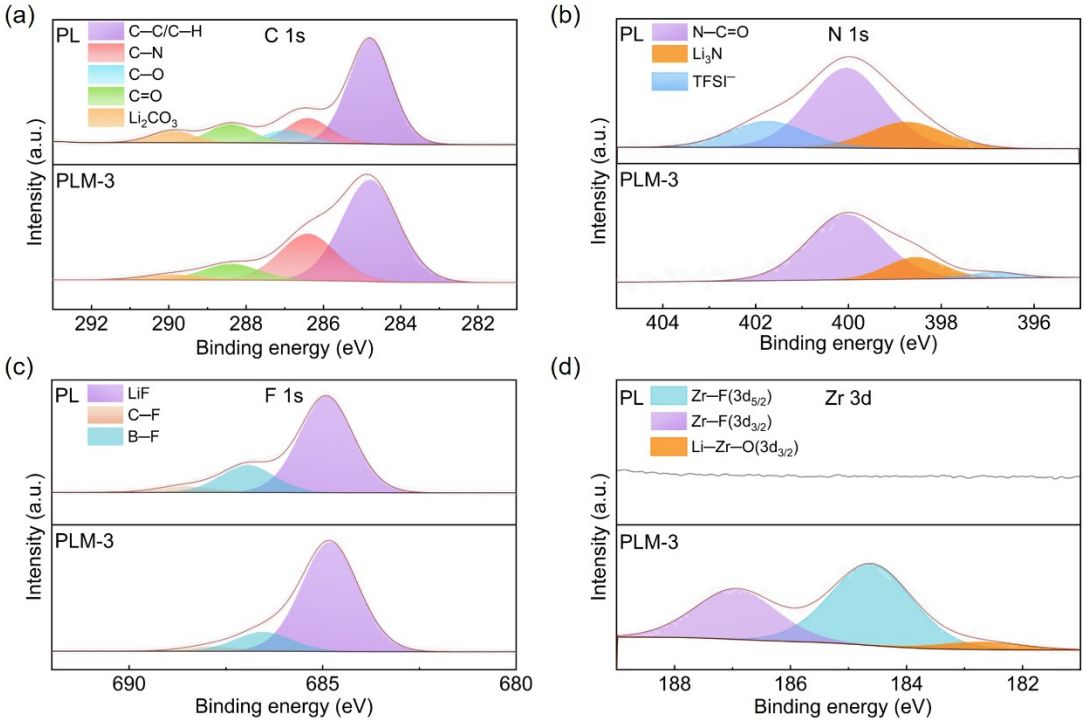

Figure S18. XPS spectrum for (a) C 1s, (b) N 1s, (c) F 1s and (d) Zr 3d of the cycled Li metal anode surface with PL and PLM-3 electrolytes.

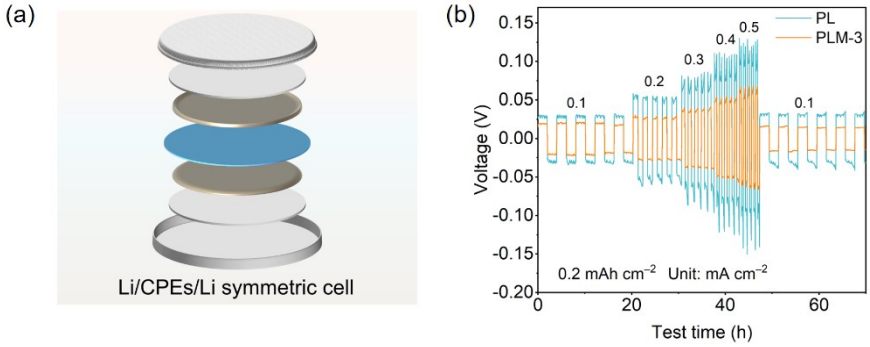

Figure S19. (a) Structure model of the Li/CPEs/Li symmetrical cells. (b) Galvanostatic charge/discharge performance of Li/CPEs/Li symmetric cells with PL and PLM-3 at different current densities (0.1, 0.2, 0.3, 0.4 and 0.5 mA cm^{-2}) and 0.2 mAh cm^{-2}.

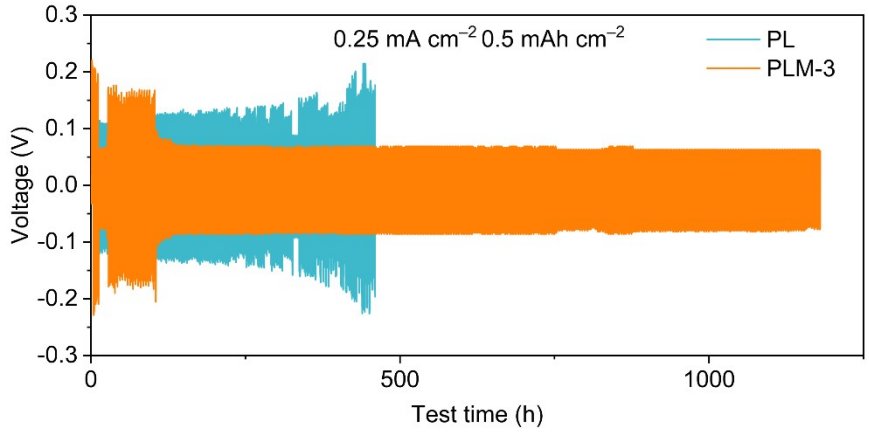

Figure S20. Galvanostatic charge/discharge performance of Li/CPEs/Li symmetric cells with PL and PLM-3 at a current density of 0.25 mA cm^{-2}.

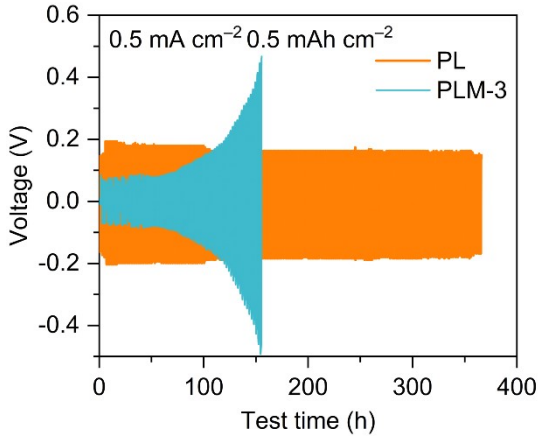

Figure S21. Galvanostatic charge/discharge performance of Li/CPEs/Li symmetric cells with PL and PLM-3 at a current density of 0.5 mA cm^{-2}.

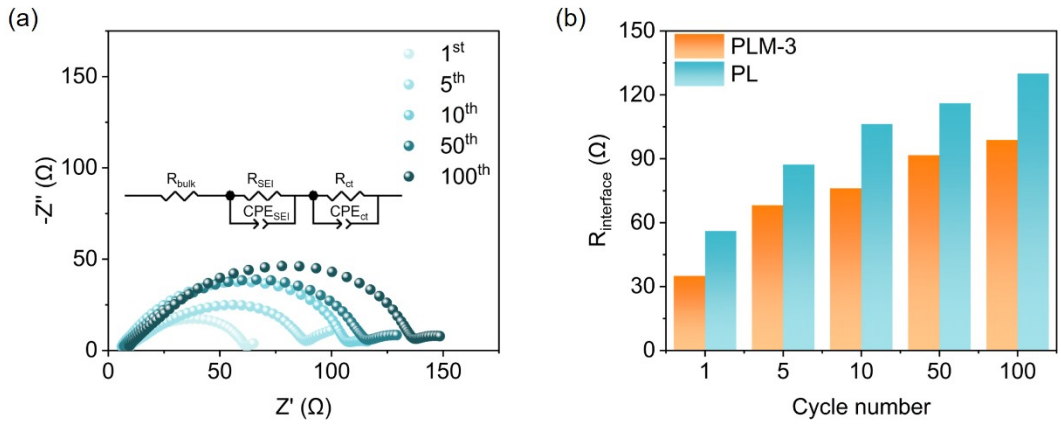

Figure S22. (a) Nyquist plots of Li/PLM-3/Li symmetric cells after 100 cycles. (b) Interfacial impedance decoupling analysis of Li/CPEs/Li cells with PL and PLM-3 electrolytes.

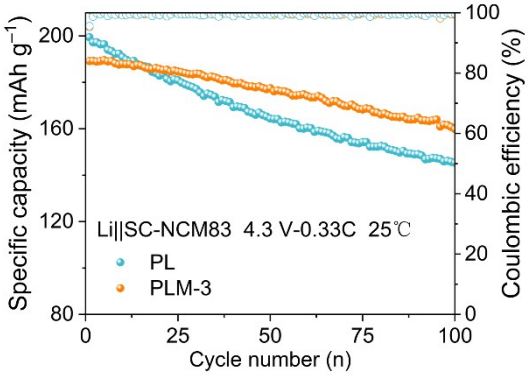

Figure S23. Cycling performance of SC-NCM83/PL/Li and SC-NCM83/PLM-3/Li cells at 0.33 C and 25 ℃ between 2.7-4.3 V.

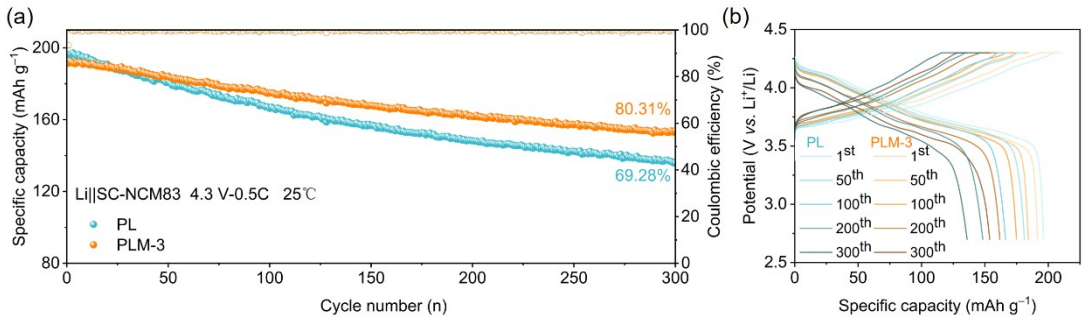

Figure S24. (a) Cycling performance of SC-NCM83/CPEs/Li cells at 0.5 C and 25 ℃ between 2.7-4.3 V. (b) Charge and discharge curves of SC-NCM83/CPEs/Li cells at 0.5 C and 25 ℃ between 2.7-4.3 V.

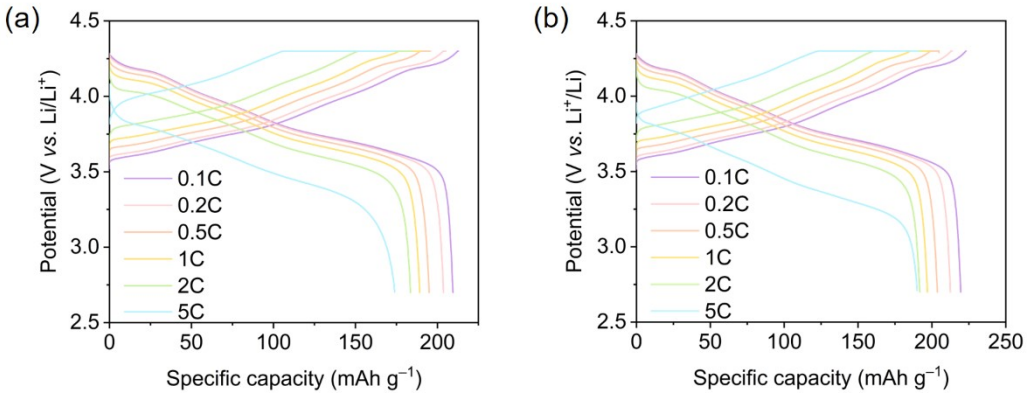

Figure S25. Charge and discharge curves at different rates of (a) SC-NCM83/PL/Li and (b) SC-NCM83/PLM-3/Li cells.

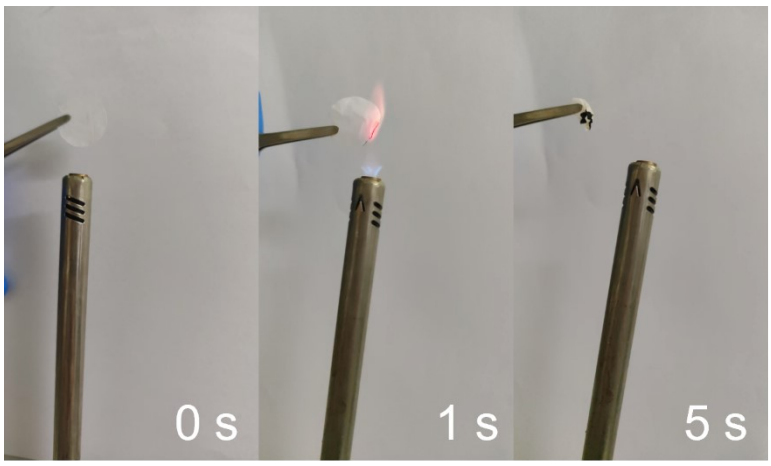

Figure S26. Flame retardancy test of PLM-3 electrolyte.

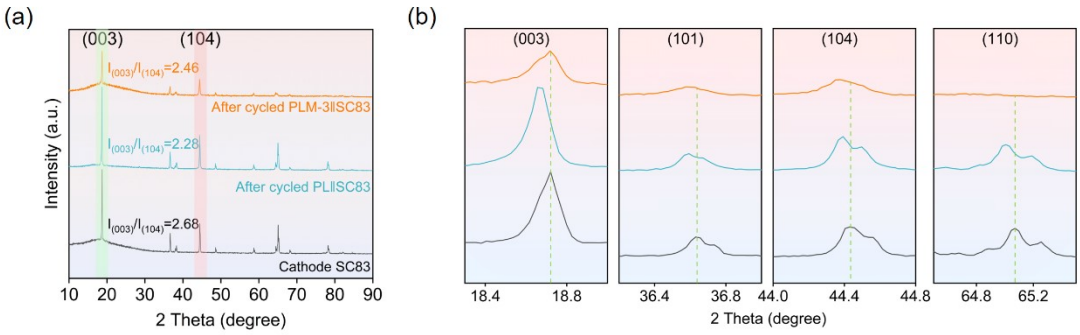

Figure S27. (a, b) XRD patterns of pristine and cycled SC-NCM83 cathodes in PL and PLM-3 electrolytes.

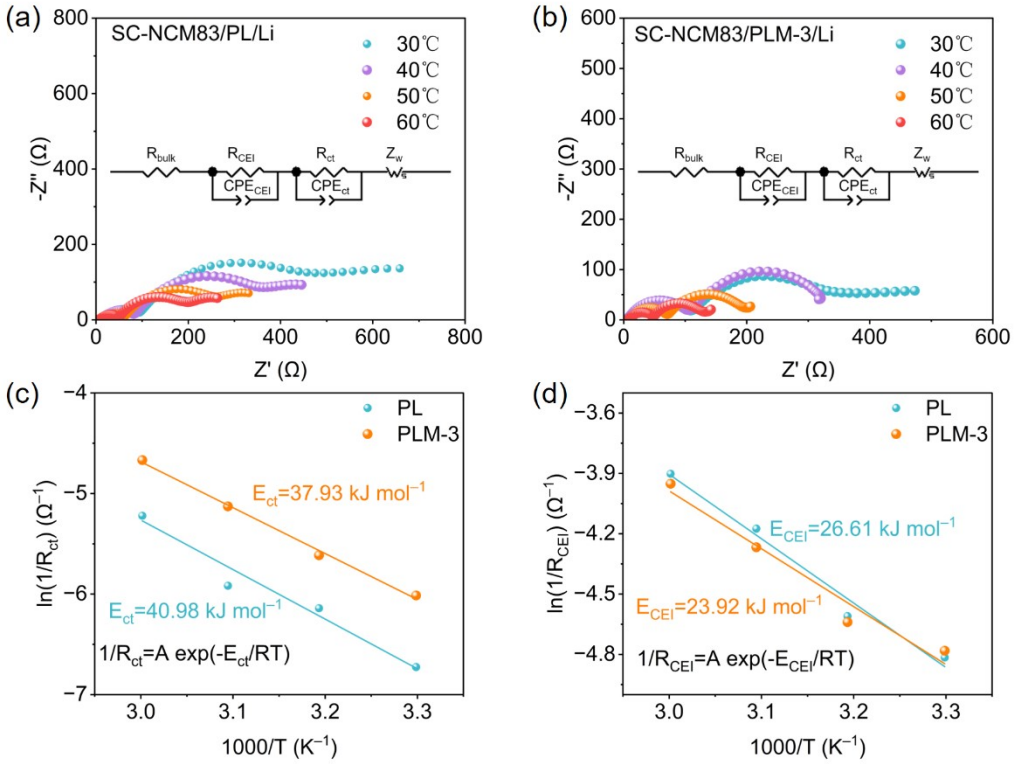

Figure S28. Nyquist plots under different temperature for (a) Li||PL||SC-NCM83 and (b) Li||PLM-3||SC-NCM83 cells after 5 cycles. The insets represent the corresponding equivalent circuit. Activation energies of (c) Li^+ desolvation process (E_{ct}) and (d) diffusion through CEI (E_{CEI}) calculated from EIS curves.

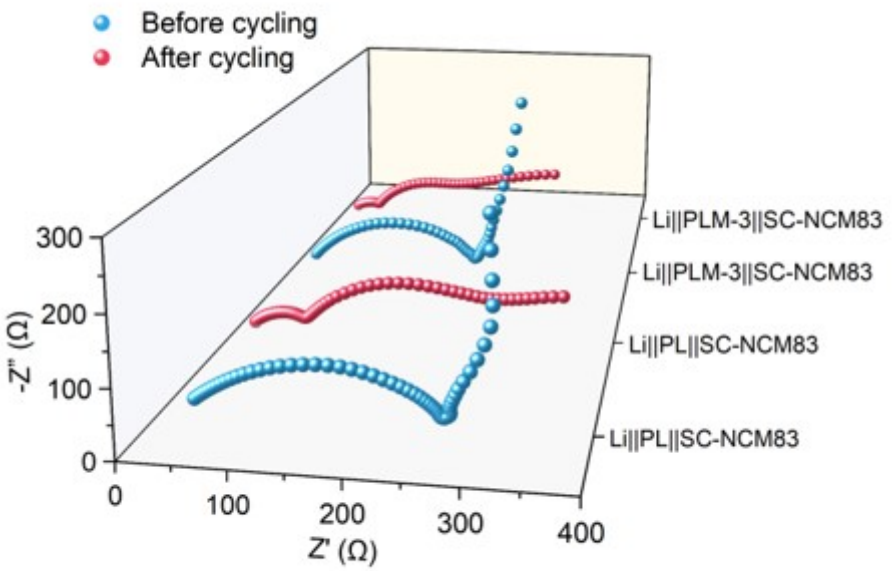

Figure S29. EIS of Li||PL||SC-NCM83 and Li||PLM-3||SC-NCM83 cells before and after cycling at 1 C.

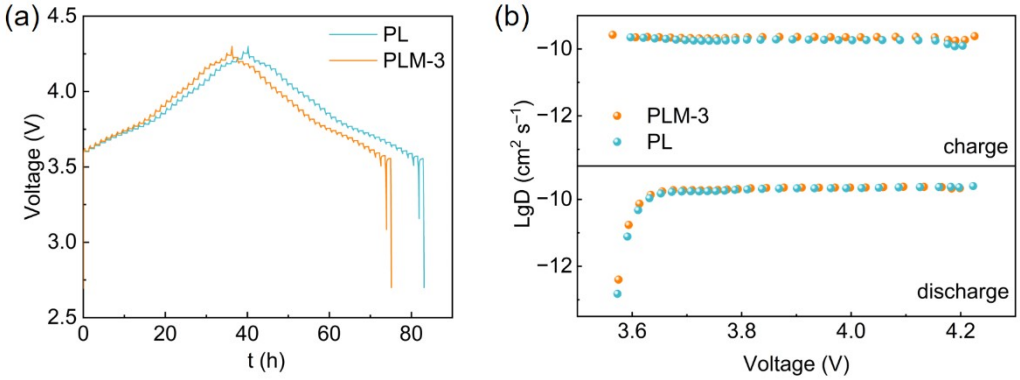

Figure S30. (a) Charge and discharge curves of GITT measurements conducted after 50 cycles and (b) corresponding D_{Li+} of SC-NCM83 cathode in PL and PLM-3.

Table S1 Cycle performance of Li||Li cell with PLM-3 compared to previous reports

CPEs composition	Li-Li battery performance	Ref.
PLM-3	0.1 mA cm^{-2}-0.1 mAh cm^{-2} for 3200 h 0.2 mA cm^{-2}-0.2 mAh cm^{-2} for 2100 h 0.5 mA cm^{-2}-0.5 mAh cm^{-2} for 350 h	This work
P(VDF–TrFE–CTFE)-LiTFSI	0.05 mA cm^{-2}-0.05 mAh cm^{-2} for 1200 h	6
PVDF-LiTFSI-LiDFOB-$LiBF_4$	0.05 mA cm^{-2}-0.05 mAh cm^{-2} for 1800 h 0.25 mA cm^{-2}-0.25 mAh cm^{-2} for 270 h	7
PVDF-LiTFSI-2D fluorinated graphene	0.1 mA cm^{-2}-0.1 mAh cm^{-2} for 900 h 0.2 mA cm^{-2}-0.1 mAh cm^{-2} for 500 h 0.5 mA cm^{-2}-0.5 mAh cm^{-2} for 340 h	8
PVDF-LiFSI-BTO/LLTO	0.1 mA cm^{-2}-0.1 mAh cm^{-2} for 1900 h 1.0 mA cm^{-2}-1.0 mAh cm^{-2} for 300 h	9
PVDF-LiFSI-LATP nanowires	0.1 mA cm^{-2}-0.1 mAh cm^{-2} for 2600 h	10
PVDF-HFP-LiTFSI-hydroxide nanosheets	0.1 mA cm^{-2}-0.05 mAh cm^{-2} for 900 h	11
PVDF-LiTFSI-LLZTO@PDA	0.1 mA cm^{-2}-0.1 mAh cm^{-2} for 1000 h	12
PVDF-HFP-LiTFSI-LLZNO nanowires/MOFs particles	0.25 mA cm^{-2}-0.125 mAh cm^{-2} for 1700 h	13
PVDF-HFP-LiFSI-LLZTO	0.3 mA cm^{-2}-0.3 mAh cm^{-2} for 240 h	14

Table S2 Cycle performance of Li||SC-NCM83 cell with PLM-3 compared to previous reports

CPEs composition	Cathode material	C-rate (C)	Cycle performance	Ref.
PLM-3	**SC-NCM83**	**0.5**	**80.31%, 300th**	**This work**
		1	**93.73%, 200th**	
polyDOL-PIC80	NCM811	0.1	74.7%, 80th	15
PVDF-HFP-LiTFSI	NCM523	1	94.5%, 200th	16
PEO-LiTFSI-3D MoO_3	NCM811	1	84.5%, 100th	17
PEO-SNFs@MMT_x	NCM811	0.5	82.5%, 180th	18
PPC-LiTFSI-Al_2O_3	NCM622	0.5	91.8%, 100th	19
PVDF-HFP-LLZTO-LiTFSI	NCM811	0.5	80.4%, 150th	20
PVDF-HFP-Li-MMT	NCM523	0.5	90%, 100th	21
PVDF-HFP-LLZTO-LiFSI	NCM811	0.5	90%, 100th	14
PVDF-d-HNTs-LiTFSI	NCM811	1	85%, 100th	22
PVDF-PMMA-BC-$BaTiO_3$-LiFSI	NCM811	0.5	80%, 200th	23

References

1 J. Li, H. Huang, W. Xue, K. Sun, X. Song, C. Wu, L. Nie, Y. Li, C. Liu, Y. Pan, H.-L. Jiang, D. Mei and C. Zhong, *Nat. Catal.*, 2021, **4**, 719-729.

2 Y. Feng, Z. Huang, R. Zhang, B. Zhong, Z. Wu, Y. Fan, Z. Yan, K. Zhang and J. Chen, *CCS Chem.*, 2025, **7**, 798-806.

3 T. Lu and F. Chen, *J. Comput. Chem.*, 2011, **33**, 580-592.

4 L. Martínez, R. Andrade, E. G. Birgin and J. M. Martínez, *J. Comput. Chem.*, 2009, **30**, 2157-2164.

5 A. V. Marenich, C. J. Cramer and D. G. Truhlar, *J. Phys. Chem. B*, 2009, **113**, 6378-6396.

6 Y.-F. Huang, T. Gu, G. Rui, P. Shi, W. Fu, L. Chen, X. Liu, J. Zeng, B. Kang, Z. Yan, F. J. Stadler, L. Zhu, F. Kang and Y.-B. He, *Energy Environ. Sci.*, 2021, **14**, 6021-6029.

7 M. Li, H. An, Y. Song, Q. Liu, J. Wang, H. Huo, S. Lou and J. Wang, *J. Am. Chem. Soc.*, 2023, **145**, 25632-25642.

8 P. Zhai, Z. Yang, Y. Wei, X. Guo and Y. Gong, *Adv. Energy Mater.*, 2022, **12**, 2200967.

9 P. Shi, J. Ma, M. Liu, S. Guo, Y. Huang, S. Wang, L. Zhang, L. Chen, K. Yang, X. Liu, Y. Li, X. An, D. Zhang, X. Cheng, Q. Li, W. Lv, G. Zhong, Y.-B. He and F. Kang, *Nat. Nanotechnol.*, 2023, **18**, 602-610.

10 K. Yang, L. Chen, J. Ma, C. Lai, Y. Huang, J. Mi, J. Biao, D. Zhang, P. Shi, H. Xia, G. Zhong, F. Kang and Y. B. He, *Angew. Chem. Int. Ed.*, 2021, **60**, 24668-24675.

11 S. Xia, B. Yang, H. Zhang, J. Yang, W. Liu and S. Zheng, *Adv. Funct. Mater.*, 2021, **31**, 2101168.

12 Y. Xu, K. Wang, X. Zhang, Y. Ma, Q. Peng, Y. Gong, S. Yi, H. Guo, X. Zhang, X. Sun, H. Gao, S. Xin, Y. G. Guo and Y. Ma, *Adv. Energy Mater.*, 2023, **13**, 2204377.

13 J. Sun, X. Yao, Y. Li, Q. Zhang, C. Hou, Q. Shi and H. Wang, *Adv. Energy Mater.*, 2020, **10**, 2000709.

14 J. Zhang, Y. Zeng, Q. Li, Z. Tang, D. Sun, D. Huang, L. Zhao, Y. Tang and H. Wang, *Energy Storage Mater.*, 2023, **54**, 440-449.

15 J. Yu, G. Zhou, Y. Li, Y. Wang, D. Chen and F. Ciucci, *Small*, 2023, **19**, 2302691.

16 W. Liu, C. Yi, L. Li, S. Liu, Q. Gui, D. Ba, Y. Li, D. Peng and J. Liu, *Angew. Chem. Int. Ed.*, 2021, **60**, 12931-12940.

17 X. Wang, S. Huang, K. Guo, Y. Min and Q. Xu, *Adv. Funct. Mater.*, 2022, **32**, 2206976.

18 W. Wang, Y. Yang, J. Yang and J. Zhang, *Angew. Chem. Int. Ed.*, 2024, **63**, e202400091.

19 X.-y. Hu, M.-x. Jing, H. Yang, Q.-y. Liu, F. Chen, W.-y. Yuan, L. Kang, D.-h. Li and X.-q. Shen, *J. Colloid Interface Sci.*, 2021, **590**, 50-59.

20 X. Yi, Y. Guo, S. Chi, S. Pan, C. Geng, M. Li, Z. Li, W. Lv, S. Wu and Q. H. Yang, *Adv. Funct. Mater.*, 2023, **33**, 2303574.

21 L. Wang, S. Yi, Q. Liu, Y. Li, Y. Hu, H. Tu, Y. Wang, A. Sun, F. Zhu, F. Mushtaq, B. Liu, P. Xue, W. Li and M. Liu, *Energy Storage Mater.*, 2023, **63**, 102961.

22 S. Lv, X. He, Z. Ji, S. Yang, L. Feng, X. Fu, W. Yang and Y. Wang, *Adv. Energy Mater.*, 2023, **13**, 2302711.

23 F. Tao, K. Yan, C. Dong, J. Wang, Q. Pan, M. Gong, J. Gu, C. Shen, R. Yu, Y. Jiang, M. Yuan, C. Zhou, M. Huang, X. Xu and L. Mai, *Angew. Chem. Int. Ed.*, 2025, **64**, e202503037.